Article

Singling out the Electrochemistry of Individual Single-Walled Carbon Nanotubes in Solution

Demis Paolucci, Manuel Melle Franco, Matteo Iurlo, Massimo Marcaccio, Maurizio Prato, Francesco Zerbetto, Alain Pe#nicaud, and Francesco Paolucci

J. Am. Chem. Soc., **2008**, 130 (23), 7393-7399 • DOI: 10.1021/ja710625p • Publication Date (Web): 14 May 2008

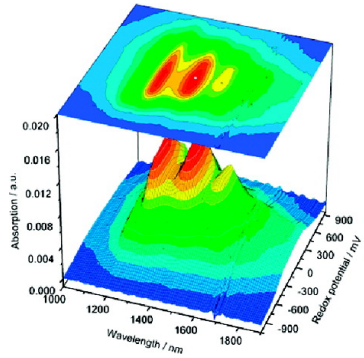

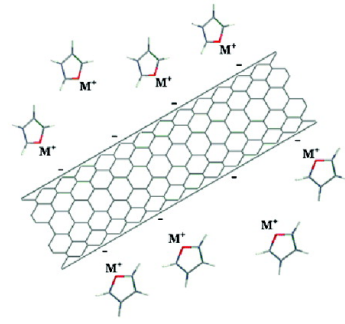

More About This Article

Additional resources and features associated with this article are available within the HTML version:

- Supporting Information
- Links to the 3 articles that cite this article, as of the time of this article download
- Access to high resolution figures
- Links to articles and content related to this article
- Copyright permission to reproduce figures and/or text from this article

View the Full Text HTML

J|A|C|S
ARTICLES

Published on Web 05/14/2008

Singling out the Electrochemistry of Individual Single-Walled Carbon Nanotubes in Solution

Demis Paolucci,*,‡ Manuel Melle Franco,‡ Matteo Iurlo,‡ Massimo Marcaccio,‡ Maurizio Prato,† Francesco Zerbetto,‡ Alain Pénicaud,§ and Francesco Paolucci*,‡

INSTM, Unit of Bologna, Dipartimento di Chimica, Università di Bologna, Via Selmi 2, I-40126 Bologna, Italy, INSTM, Unit of Trieste, Dipartimento di Scienze Farmaceutiche, Università di Trieste, Piazzale Europa, 1, I-34127 Trieste, Italy and Centre de Recherche Paul Pascal-CNRS, Université Bordeaux-I, AV. Schweitzer, 33600 Pessac, France

Received November 27, 2007; E-mail: francesco.paolucci@unibo.it

Abstract: Bandgap fluorescence spectroscopy of aqueous, micelle-like suspensions of SWNTs has given access to the electronic energies of individual semiconducting SWNTs, while substantially lower is the success achieved in the determination of the redox properties of SWNTs as individual entities. Here we report an extensive voltammetric and vis-NIR spectroelectrochemical investigation of true solutions of unfunctionalized SWNTs and determine the standard electrochemical potentials of reduction and oxidation as a function of the tube diameter of a large number of semiconducting SWNTs. We also establish the Fermi energy and the exciton binding energy for individual tubes in solution. The linear correlation found between the potentials and the optical transition energies is quantified in two simple equations that allow one to calculate the redox potentials of SWNTs that are insufficiently abundant or absent in the samples.

Introduction

The properties of single wall carbon nanotubes (SWNTs) depend markedly on their diameter and helicity. In the bulk phase, the identification of specific quantities relative to individual tubes is notoriously challenging and requires extreme ingenuity, as in the case of bandgap fluorescence spectroscopy of aqueous, micelle-like suspensions of SWNTs that has given access to the electronic energies of individual semiconducting SWNTs.[1] Substantially lower is the success achieved in the determination of the redox properties of SWNTs[2,3] that are necessary to design the fabrication and/or the integration of the tubes into, for example, electroluminescent or other (opto)electronic practical devices. Some data, as a function of the electrode potential, are available.[4–6] The *n*- and *p*-doping bleaches the intra-gap transitions (and the Raman radial breathing modes) allowing a determination of the redox levels of a few semiconducting SWNTs supported onto solid electrodes.[7–9] However, the strong tube−tube and tube−substrate interactions gave poorly resolved spectra, without proper matching of specific optical transitions to individual SWNTs. The difficulty of performing proper *solution* spectro-electrochemical experiments able to gain information on individual nanotubes is associated with (i) the high ionic strength typical of electrochemical experiments (due to the addition of a supporting electrolyte) that promotes flocculation of the SWNT suspension, (ii) the interference, with the electrochemical experiment, of the surfactants used to solvate the SWNT that foul the working electrodes, and (iii) the limited electrochemical stability window of the aqueous medium. These difficulties are minimized by a recently reported, innovative way to form thermodynamically stable solutions of unmodified and uncut SWNTs.[10] Upon reduction with alkali metals, SWNTs produce polyelectrolyte salts (Scheme 1) that are soluble in polar organic solvents without use of sonication, surfactants, or functionalization.

Here, we report an extensive vis-NIR spectroelectrochemical investigation of true solutions of unfunctionalized SWNTs that allowed the determination of the standard redox potentials of individual semiconducting SWNTs as a function of the tube structure. Both the reduction and the oxidation of each SWNT were independently investigated, and the Fermi energy and the exciton binding energy of the individual tubes in solution were also established.

Voltammetry. Polyelectrolyte SWNT salts were obtained by reacting arc-discharge samples (***a*-NT**) or HiPco samples (***h*-NT**) with different alkali metals (Na, K).[10] Oxygen free solutions were then prepared for electrochemical investigations in ultradry DMSO. To avoid flocculation of the SWNTs, low concentrations

‡ Università di Bologna.
† Università di Trieste.
§ Université Bordeaux.

(1) Bachilo, S. M.; Strano, M. S.; Kittrell, C.; Hauge, R. H.; Smalley, R. E.; Weisman, R. B. *Science* **2002**, *298*, 2361.
(2) O'Connell, M. J.; Eibergen, E. E.; Doorn, S. K. *Nat. Mater.* **2005**, *4*, 412.
(3) Zheng, M.; Diner, B. A. J. *Am. Chem. Soc.* **2004**, *126*, 15490.
(4) Rafailov, P. M.; Maultzsch, J.; Thomsen, C.; Kataura, H. *Phys. Rev. B* **2005**, *72*, 045411.
(5) Kavan, L.; Dunsch, L. *ChemPhysChem* **2007**, *8*, 974.
(6) Kazaoui, S.; Minami, N.; Matsuda, N.; Kataura, H.; Achiba, Y. *Appl. Phys. Lett.* **2001**, *78*, 3433.
(7) Kavan, L.; Rapta, P.; Dunsch, L.; Bronikowski, M. J.; Willis, P.; Smalley, R. E. J. *Phys. Chem. B* **2001**, *105*, 10764.
(8) Corio, P.; Jorio, A.; Demir, N.; Dresselhaus, M. S. *Chem. Phys. Lett.* **2004**, *392*, 396.
(9) Okazaki, K.; Nakato, Y.; Murakoshi, K. *Phys. Rev. B* **2003**, *68*, 035434.
(10) Pénicaud, A.; Poulin, P.; Derré, A.; Anglaret, E.; Petit, P. J. *Am. Chem. Soc.* **2005**, *127*, 8.

Scheme 1. Cartoon Structure of the Soluble SWNTs Salts $M^+(THF)C_n$ of This Work. $M^+ = Na^+, K^+$

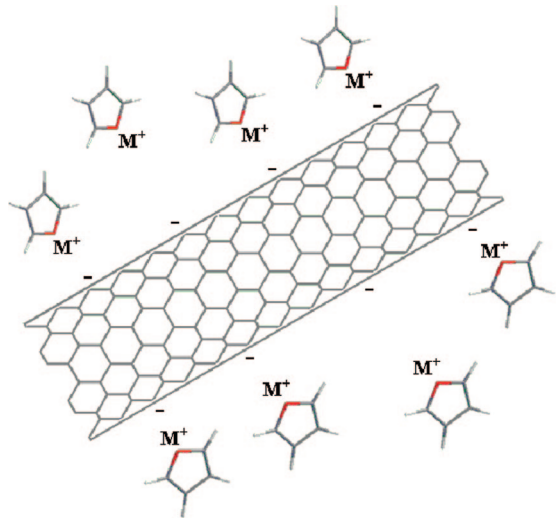

of the supporting electrolyte (tetrabutylammonium hexafluorophosphate, TBAH) were used. The open circuit potential (OCP) measured at the platinum electrode, after equilibration with the intact, initial solution, was −0.40 V. This value is significantly more negative than the OCP of neutral SWNTs,[7] in agreement with the presence of reduced SWNTs in the solution. Figure 1a shows the cyclic voltammetric (CV) curve of a saturated DMSO solution of Na[***a*-NT**], obtained scanning the potential from the OCP toward more negative values.

The curve displays a continuum of current due to the progressive filling of the electronic bands of the SWNTs. A similar behavior was also found for Na[***h*-NT**] (not shown) and resembles that of pyrrolidine-functionalized SWNT, ***f*-NT** (see Supporting Information, Scheme S1), investigated under similar conditions.[11,12] The more detailed comparison of the curves at potentials closer to the OCP (Figure 1b) shows that (i) the current onset is anticipated for Na[***a*-NT**] with respect to Na[***h*-NT**] and to the ***f*-NT** that were also produced from HiPco NTs; (ii) the curves of ***h*-NT** and ***a*-NT** (for both K^+ and Na^+ salts) are richer in structure than that of ***f*-NT**. In particular, the broad waves at −0.81 and −1.05 V (***h*-NT**) and −0.56 and −0.99 V (***a*-NT**) are missing for ***f*-NT**. The anticipated onset is indicative of a smaller energy gap, consistent with the larger average diameters of the arc-SWNTs with respect to the HiPco ones. The richer curve morphology reflects, instead, the more complex electronic structure of the pristine materials, compared with ***f*-NT**, in agreement with recent calculations which suggested that functionalization significantly affects the low lying electronic states of the nanotubes.[11] The broad irreversible anodic peak observed at ca. −0.6 V in the reverse CV scan in Figure 1a is associated with the oxidative stripping of an alkali metal (Na) film that forms onto the electrode during the forward scan, at potentials less than or equal to −2.2 V.

Visible-NIR Spectroelectrochemistry. The spectroelectrochemical investigation of the ***h*-NT** and ***a*-NT** solutions was carried out in the ±1500 mV range (vs SCE). The selection of

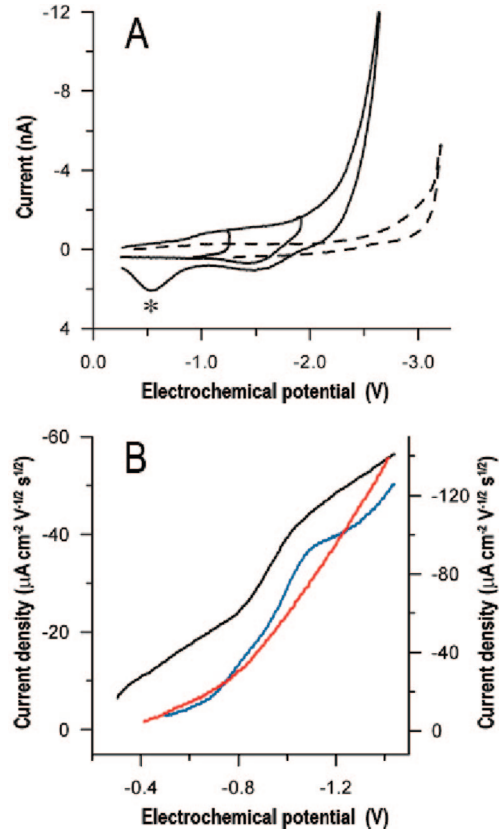

Figure 1. (a) CV curve of a DMSO solution saturated with Na[**a-NT**] (full line) compared to the response of the blank, supporting electrolyte, solution (dashed line). The star indicates the irreversible anodic peak in the reverse CV scan, which is due to the oxidative stripping of the reduced alkali metal film. (b) Details of the current onsets: black line for saturated Na[***a*-NT**] solution; blue line for saturated Na[***h*-NT**]; red line for saturated ***f*-NT** solution. The black and blue curves are referred to the left axis, the red curve to the right axis. Experimental conditions: NT solution in 2 mM TBAH/DMSO; working electrode Pt disk ($r = 25$ μm); data recorded at 298 K; scan rate 1 Vs^{-1}. Potentials are referenced to SCE.

the negative limit is due to the formation of the metal film onto the electrode surface, while the highest potential was limited by the solvent stability. In the positive oxidizing range, the solutions of electrochemically neutralized SWNTs are remarkably stable. No flocculation was observed in the time scale of the experiment. Doping modifies the population of the first and second van Hove singularities of the electronic bands of SWNTs and the electronic transitions affected by charging are the semiconducting S_{11} ($\upsilon_s^1 \rightarrow c_s^1$) and S_{22} ($\upsilon_s^2 \rightarrow c_s^2$) and possibly the metallic M_{11} ($\upsilon_m^1 \rightarrow c_m^1$).[13] The higher spectral resolution in the case of ***h*-NT** and their complete bleaching achieved in the range of the working potentials made us focus the analysis on the more intense S_{11} transitions.

As expected for heavily *n*-doped SWNTs, the starting solutions do not show significant absorption and only the plasmon band, typical of graphitic materials, is present.[14,15] No spectral change was recorded as long as the applied potential

(11) Melle-Franco, M.; Marcaccio, M.; Paolucci, D.; Paolucci, F.; Georgakilas, V.; Guldi, D. M.; Prato, M.; Zerbetto, F. J. *Am. Chem. Soc.* **2004**, *126*, 1646.
(12) Guldi, D. M.; Marcaccio, M.; Paolucci, D.; Paolucci, F.; Tagmatarchis, N.; Tasis, D.; Vázquez, E.; Prato, M. *Angew. Chem., Int. Ed.* **2003**, *42*, 4206.
(13) Saito, R.; Dresselhaus, G.; Dresselhaus, M. S. *Phys. Rev. B* **2000**, *61*, 2981.
(14) Pichler, T.; Knupfer, M.; Golden, M. S.; Fink, J.; Rinzler, A.; Smalley, R. E. *Phys. Rev. Lett.* **1998**, *80*, 4729.
(15) (a) Petit, P.; Mathis, C.; Journet, C.; Bernier, P. *Chem. Phys. Lett.* **1999**, *305*, 370. (b) Niyogi, S.; Hamon, M. A.; Hu, H.; Zhao, B.; Bhowmik, P.; Sen, R.; Itkis, M. E.; Haddon, C. *Acc. Chem. Res.* **2002**, *35*, 1105.

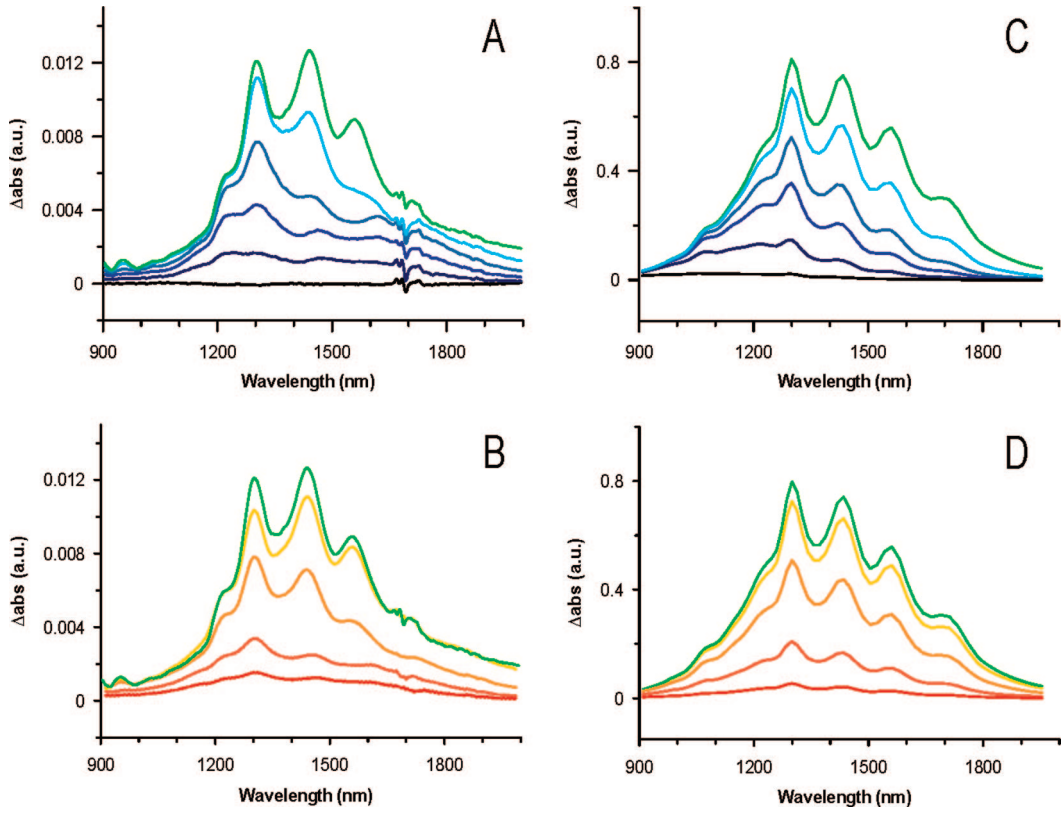

Figure 2. Difference absorption spectra of DMSO solutions, recorded during the spectroelectrochemical experiments (the reference spectrum corresponds to the highly reduced state, at $E = -1450$ mV): (a) S_{11} transitions of *n*-doped K[***h*-NT**] at −1050, −800, −650, −550, −400, and −50 mV (from black to the green lines). (b) S_{11} transitions of p-doped K[***h*-NT**] at +950, +700, +450, +200, and −50 mV (from red to the green line). Experimental conditions: 2 mM TBAH, saturated DMSO solution, $T = 298$ K. Potentials referenced to SCE. (c,d) Simulations (for details see text) of the spectra at the potentials used on the left.

was less than or equal to −1.2 V. At less negative potentials, changes appeared in the absorption spectra associated with the progressive undoping of SWNTs. Figure 2 panels a and b display the spectral evolution of DMSO solutions of $[\boldsymbol{h}\text{-NT}]^{n-}$.

The S_{11} transitions start appearing at $E \geq -1.2$ V and their intensity increases progressively until the maximum is reached for the complete depletion of the conduction bands. All spectral modifications are reversible with the applied potential. This indicates the existence of an equilibrium between the populations of the variously doped SWNTs and implies the stability of materials in the various charged states. The electronic bands in Figure 2a,b are red-shifted by 35 meV with respect to a dispersion of pristine HiPco in D_2O with sodium dodecyl sulfate (SDS).[16,17] This is due to the diverse dielectric environment, possibly in combination with some differences in the degree of aggregation.[17,18] In fact, as a check, the K[**h-NT**] sample was dried, washed with HCl,[19] and suspended in SDS/D_2O. The absorption spectrum was blue-shifted by 15 meV, with respect to DMSO solutions, and closely matched those shown in Figure 2a,b (see Supporting Information, Figure S1).

The $[\boldsymbol{a}\text{-NT}]^{n-}$ solution behaves similarly. However, to larger tube diameters correspond electronic transitions that occur at lower energy, with the important finding that the electrochemical undoping discovers the M_{11} transitions too (see Supporting Information, Figure S2). In line with the reported behavior of arc-discharge SWNTs,[15] the closely spaced S_{11} transitions give rise—in this case—to a poorly resolved band, that is, moreover, partly distorted by the strong solvent absorption band occurring at ca. 1700 nm (Figure S2). A summary of the spectroelectrochemical investigation of ***h*-NT** is shown in the contour plot of Figure 3a.

On both reduction and oxidation sides, the absorption bands have different onset potentials. As expected qualitatively, the transitions at higher energy recover their intensity at higher potentials (either more negative or more positive) than those at lower energy.

Analysis of the Measurements. For sake of simplicity we make the hypotheses that the absorbance is due only to neutral SWNTs (and that they do it according to Lambert−Beer law), and that the Nernst equation describes the ratios of activity (concentration) of the neutral-to-reduced (or -oxidized) SWNTs. Therefore the absorbance (A) of the samples is described as a function of electrochemical potential by two equations for the *n*-doped and *p*-doped SWNTs:

$$A_{n-\mathrm{dop},i} = \varepsilon_{N,i} b c_i^* \frac{\exp\left(\frac{F}{RT}\left(E - E^0_{\mathrm{red},i}\right)\right)}{1 + \exp\left(\frac{F}{RT}\left(E - E^0_{\mathrm{red},i}\right)\right)};$$

$$A_{p-\mathrm{dop},i} = \varepsilon_{N,i} b c_i^* \frac{1}{1 + \exp\left(\frac{F}{RT}\left(E - E^0_{\mathrm{ox},i}\right)\right)} \quad (1)$$

(16) Weisman, R. B.; Bachilo, S. M. *Nano Lett.* **2003**, *3*, 1235.
(17) O'Connell, M. J.; Bachilo, S. M.; Huffman, C. B.; Moore, V. C.; Strano, M. S.; Haroz, E. H.; Rialon, K. L.; Boul, P. J.; Noon, W. H.; Kittrell, C.; Ma, J.; Hauge, R. H.; Weisman, R. B.; Smalley, R. E. *Science* **2002**, *297*, 593.
(18) Ohno, Y.; Iwasaki, S.; Murakami, Y.; Kishimoto, S.; Maruyama, S.; Mizutani, T. *Phys. Rev. B* **2006**, *73*, 235427.

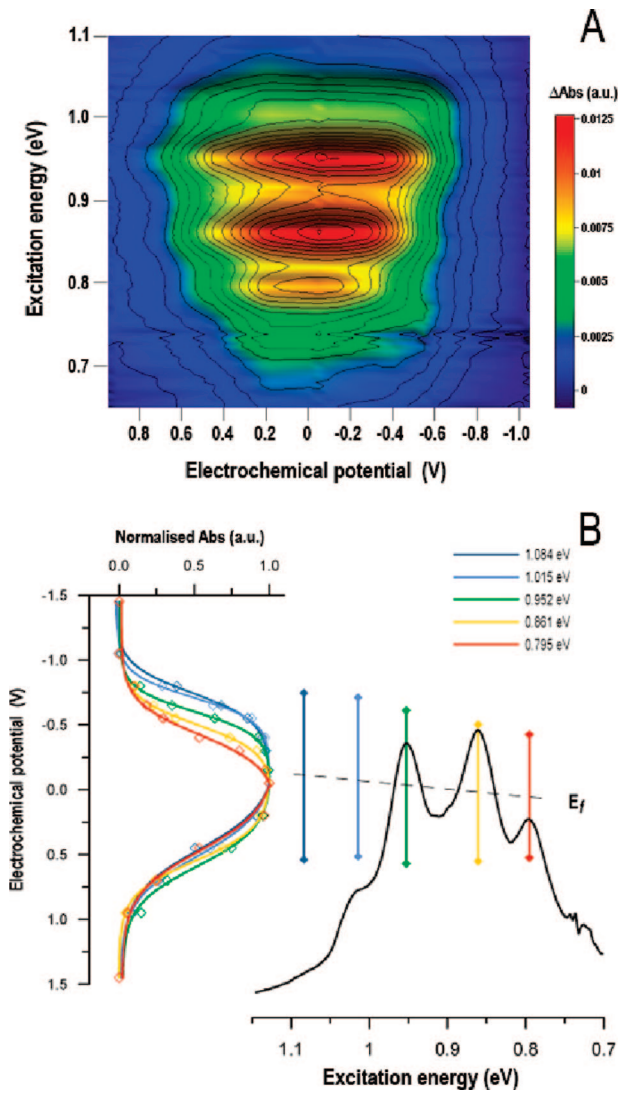

Figure 3. (a) Contour plot showing the spectral evolution in the S_{11} region as a function of potential for K[**h-NT**]. Absorption intensities reach their maximum value for electrochemical potentials around zero and decrease at higher (and lower) electrochemical potentials. (b) (Left) The intensity of each of the five bands selected in the spectrum shown on the right was normalized by its maximum value and plotted vs potential. The fitting curves (full lines) were calculated using eqs 1, where $E^0_{ox,i}$ and $E^0_{red,i}$ values were obtained (corresponding to the inflection points in each sigmoidal curve). (Right) absorption spectrum of K[***h*-NT**] at −50 mV. The vertical bars represent the (average) electrochemical gaps (i.e., $E^0_{ox,i} - E^0_{red,i}$) of all the NTs pertaining to the corresponding absorption band. Its midpoint is indicated as the Fermi level of such NTs. In all plots raw electrochemical data, that is, uncorrected for ohmic drop, are referenced to SCE (see Table 1 for corrected data).

where i is a single (n,m) nanotube that contributes to a specific transition band, ε_N is the extinction coefficient of the neutral (n,m) nanotube (for simplicity assumed to be the same for all tubes), c* is its bulk concentration, E is the electrochemical potential, b is the path of the spectroscopic cell, and $E_{red,i}$ and $E_{ox,i}$ are the standard potentials of its reduction (n-doping) and oxidation (p-doping).[20]

Table 1. Electrochemical and Optical Data for Unmodified SWNTs[a]

E_{exc}[b]/eV	E_{ox}[c]/eV	E_{red}[c]/eV	E_{gap}/eV	E_{bind}[d]/eV	assignment[e]
1.084	0.575	−0.840	1.415	0.331	(9,4) (8,4) (7,6)
1.015	0.550	−0.806	1.356	0.341	(8,6) (12,1) (11,3)
0.953	0.606	−0.705	1.311	0.360	(9,5) (10,3) (10,5) (8,7) (11,1)
0.861	0.587	−0.597	1.184	0.323	(12,4) (11,4) (12,2) (13,0) (9,8)
0.795	0.541	−0.540	1.081	0.286	(13,3) (12,5) (14,1)
0.760	0.485	−0.515	1.000	0.240	(12,7) (17,0) (10,9) (16,2)
0.743	0.483	−0.492	0.975	0.232	(11,9) (15,4)
0.726	0.470	−0.477	0.947	0.221	(14,4) (13,6) (14,6)
0.712	0.466	−0.478	0.944	0.232	(12,8)
0.701	0.458	−0.471	0.929	0.228	(13,8) (18,1) (17,3)
0.679	0.432	−0.449	0.881	0.202	(16,5) (17,1) (16,3)

[a] Data collected for saturated solution of ***h*-NT** and ***a*-NT** in 2 mM TBAH/DMSO, at 298 K. [b] Excitation energy. [c] Electrochemical standard potentials referred to SCE. Data were corrected for the ohmic drop $i_{1/2} \times R_\Omega$, where $i_{1/2}$ was the current intensity measured during the electrochemical process at the inflection point and R_Ω the uncompensated solution resistance between working and reference electrode, independently obtained by electrochemical impedance spectroscopy (see Experimental Section). [d] Exciton binding energy. [e] From ref 16, corrected by 35 meV (red-shift) for taking the solvent effects into account (see text).

After normalization, the intensity of each band in the spectra shown in the right part of Figure 3b was analyzed according to eqs (1), see left of Figure 3b, to give a set of standard potentials for the oxidations ($E_{ox,i}$) and reductions ($E_{red,i}$) of ***h*-NT**. The caption of Figure 3 gives details of the procedure, which is best illustrated graphically. An analogous procedure was carried out to obtain the corresponding standard potentials of ***a*-NT** (see Supporting Information, Figure S3).

Redox Potentials and Fermi Energies. The potentials of ***h*-NT** and ***a*-NT** are reported in Table 1 and plotted in Figure 4a as a function of the excitation energy for the S_{11}.

The E^0 values vary linearly with the excitation energy (Figure 4a). To first order, the redox potential fit the equations $E_{red} = -1.02 \times E_{exc} + 0.26$, $R^2 = 0.989$, and $E_{ox} = 0.36 \times E_{exc} + 0.22$, $R^2 = 0.704$, that can be employed in the design of devices.

The assignment of the redox potentials in Table 1 were obtained by adopting the empirical expressions of ref 16 which give the excitation energies of the van Hove optical transitions as a function of the structure for a wide range of semiconducting nanotubes. Since the data referred to an aqueous SDS suspension of SWNTs, before comparison, the excitation energies measured in DMSO were corrected by adding 35 meV (see earlier).

The energy of the Fermi level in the neutral state (E_f) was then calculated as the average of oxidation and reduction potentials (Figure 4b) and is almost constant for ***a*-NT**s, while for ***h*-NT**s it is linear with the energy of the optical gap. In line with our findings, recent calculations suggest that the work function (WF = $-E_f$) is substantially independent of diameter and chirality for larger diameter SWNTs ($d > 0.9$ nm), and it either decreases (for semiconducting tubes) or increases (for metallic tubes) with diameter, in the case of thinner ones.[21,22] Photoemission electron microscopy of individual SWNTs showed that their work functions tend to group inside a narrow range of 0.20 eV.[23] In bundles of SWNTs, the work functions

(19) Pénicaud, A.; Valat, L.; Derré, A.; Poulin, P.; Zakri, C.; Roubeau, O.; Maugey, M.; Miaudet, P.; Anglaret, E.; Petit, P.; Loiseau, A.; Enouz, S. *Comput. Sci. Technol.* **2007**, *67*, 795.
(20) Bard, A. J.; Faulkner, L. R. *Electrochemical Methods: Fundamentals and Applications*; Wiley: New York, 2001; Chapter 17.
(21) Shan, B.; Cho, K. *Phys. Rev. Lett.* **2005**, *94*, 236602.
(22) Barone, V.; Peralta, J. E.; Uddin, J.; Scuseria, G. E. J. *Chem. Phys.* **2006**, *124*, 024709.
(23) Suzuki, S.; Watanabe, Y.; Homma, Y.; Fukuba, S.-Y.; Heun, S.; Locatelli, A. *Appl. Phys. Lett.* **2004**, *85*, 127.

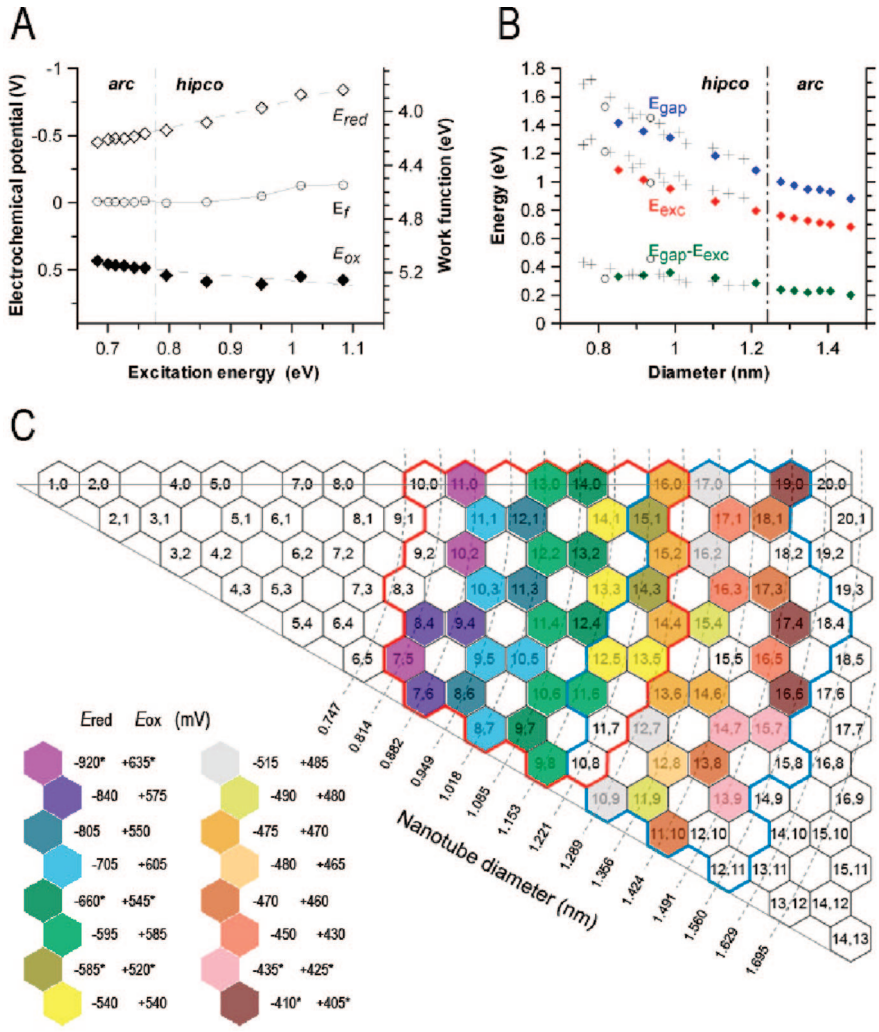

Figure 4. (a) Oxidation (solid diamonds) and reduction (open diamonds) standard potentials and Fermi levels (open circles) of semiconducting SWNTs, as a function of the excitation energy. Potential data were plotted with reference to either the SCE electrode (left axis) or the vacuum level (right axis), assuming that the latter is located at 4.68 eV with respect to SCE.[42] (b) The electrochemical gap (blue diamonds), the excitation energy (red diamonds), and the exciton binding energy (green diamonds) plotted as a function of the nanotube diameters, calculated from excitation energies according to ref 16. Also shown in the plot are data taken from ref 35 (crosses) and ref 36 (open circles). (c) Chirality map displaying the average standard potentials associated to each of the SWNT structures identified in this work. HiPco SWNTs are located inside the red line, while arc-discharge SWNT are inside the blue line. Starred values were extrapolated from the linear-fitting equations given in the text.

are between 4.6−4.8 eV,[24,25] larger than the 4.6 eV of graphite.[26] The work function values obtained here cover a range of 0.15 eV between the values of graphite and bundles. The trend is reproduced by ab initio calculations carried out in the absence of solvent (see Supporting Information, Figure S4).

The standard potentials of the SWNTs identified in this work are shown in the chirality map of Figure 4c, where color codes are used to gather the structures that share the same values. Different colors form patterns in the map which show that, in analogy with optical transition frequencies,[1] a simple dependence of redox properties of SWNTs on diameter is not strictly followed.

Consistency and Accuracy of the Results. The equations that relate potentials to excitation energies (see above) were used to calculate the potential-dependent spectra shown in Figure 2a and 2b. The relative abundances of the SWNTs present in the HiPco samples were taken from ref 27. Each abundance was weighed at each potential using eqs 1 and the corresponding E^0 values from Table 1 and Figure 4c. The final spectrum was calculated by summing up the contribution from each nanotube. The very good agreement of the simulated spectra with the experimental ones (compare Figure 2 panels a and b to Figure 2 panels c and d) vouches for the accuracy and the consistency of our analysis. In the simulations, the extinction coefficient of the neutral (n,m) nanotube were assumed for simplicity to be the same for all tubes. In the Supporting Information, Figure S5, a comparison of the spectrum obtained maintaining constant the extinction coefficients and varying them as a function of chirality and diameter[28] is provided. It shows that with the spectral line width of our experiments, the difference between the two approaches is remarkably small. A similar treatment of

(24) Suzuki, S.; Bower, C.; Watanabe, Y.; Zhou, O. *Appl. Phys. Lett.* **2000**, *76*, 4007–4009.
(25) Shiraishi, M.; Ata, M. *Carbon* **2001**, *39*, 1913.
(26) Marchand, D.; Frétigny, C.; Laguës, M.; Batallan, F.; Simon, C.; Rosenman, I.; Pinchaux, R. *Phys. Rev. B* **1984**, *30*, 4788.
(27) Kukovecz, A.; Kramberger, C.; Georgakilas, V.; Prato, M.; Kuzmany, H. *Eur. Phys. J. B* **2002**, *28*, 223.
(28) Luo, Z.; Pfefferle, L. D.; Haller, G. L.; Papadimitrakopoulos, F. *J. Am. Chem. Soc.* **2006**, *128*, 15511.

the arc-discharge potential-dependent spectra gave a much less satisfactory result in the region of the S_{11} transitions because of the accidental occurrence of a strong solvent absorption band at 1700 nm (Figure S2). Notice, however, that the analysis of intensity changes as a function of potential still allowed the determination of the relevant $E°$ values (Figure S3). The validity of the present model in the case of ***a*-NT** was confirmed by the successful simulation of the S_{22} region (Figure S6).

For each SWNT, the difference of the redox potentials represents the gap between the van Hove singularities of the electronic band structure ($E_{gap} = E_{ox} - E_{red}$). E_{gap} is larger than the excitation energy because of the Coulomb attraction experienced by the excited electron with the positive hole left in the valence band, $E_{exc} < E_{gap}$.[29] The exciton binding energy $E_{bind} = E_{gap} - E_{exc}$ is a function of the tube diameter, chirality, and environment.[30–35]

Figure 4b compares the optical gap (excitation energy) and the electrochemical one (bandgap) in DMSO as a function of nanotube diameter. It shows (see also Table 1) that the exciton binding energy is inversely proportional to the nanotube diameter and ranges from 0.36 (0.29) to 0.23 (0.20) eV for the HiPco (arc-discharge) sample. In Figure 4b, the exciton binding energy and bandgap energy of HiPco SWNTs recently measured by two-photon excitation spectroscopy are also shown[35] together with the effective energy bandgap recently evaluated by resonant Raman scattering coupled with electrochemistry for SWNT (7,5) and (10,3), that is, 1.53 and 1.45 eV, respectively.[36] These values compare rather well with our results (Figure 4b). The rather different experimental conditions used elsewhere may explain the small deviations of E_{gap} (av deviation = 34 meV) and E_{bind} (av deviation = 9 meV) with respect to our data.[18,34,37] The relatively lower deviation observed for E_{bind} agrees with the recent observation that exciton binding energies of SWNTs are not strongly affected by the dielectric properties of the medium.[38,39]

Finally, the energies of the LUMOs relative to the vacuum level of a range of semiconducting SWNTs, also comprising some of the structures investigated in this work, were recently determined using a biohybrid approach and Nernst equation.[40] The energies vary linearly with E_{red} calculated by us. This finding allows the extension of the range of structures directly investigated in this work. The energies of the LUMOs fit the linear equation (passing through origin) $E(\text{LUMO}) = 1.1 \times E_{red}$ ($R^2 = 0.9998$). Likely, the slope exceeds slightly the expected unity value because of the different media used in the two cases, that is, aqueous solutions versus organic solvent. The difference between the two sets of data is inversely proportional to the nanotube diameter (see Supporting Information, Figure S7), in line with prevalent ion−solvent interactions effects.[41]

Conclusions

The redox potentials of a large number of semiconducting nanotubes were obtained from the analysis of cyclic voltammetry and spectro-electrochemistry measurements. The linear correlation that was found to exist between the potentials and the excitonic energy was quantified in terms of two simple equations that allow to calculate the potentials of other SWNTs that are insufficiently abundant or absent in the sample. The results were checked for consistency in two independent ways. In the first, the electronic measured spectra, as a function of the potential, were accurately reproduced; in the second, the excitonic binding energy of the nanotubes obtained elsewhere were also well matched. Finally, the calculated E_{red} values also compared rather well with experimental values recently reported for some nanotubes not directly investigated in this work. The knowledge of the oxidation and reduction potentials, together with the Fermi energies that were also obtained here, paves the way to the rational design of electrochemical and electronic devices, such as sensors, light emitting diodes, or other electroluminescent devices, in which the energetics of electrochemical and electric generation of electrons and holes in the SWNTs play an important role.

Experimental Section

Materials. The HiPco SWNTs were obtained from Carbon Nanotechnologies Inc., while the arc-discharge samples were from Nanoledge. The polyelectrolyte SWNT salts were synthesized upon reaction with different alkali metals, following the procedures published in ref 10. Functionalized SWNTs were, instead, prepared according to the 1,3-dipolar cycloaddition of azomethine ylides to the nanotube sidewall, as described in ref 43. Tetrabutylammonium hexafluorophosphate (from Fluka), along with the electroactive compound, was dried into the electrochemical cell under vacuum at 370 K for at least 48 h. Ultradry dimethylsulfoxide (DMSO) was chosen as solvent due to its high capability to dissolve the SWNT salts. The commercial DMSO (purum, Fluka) was first treated with basic alumina (from MP Biomedicals) in a flask for at least 48 h. Afterward, the solvent was distilled trap-to-trap into an especially designed Schlenk, containing activated 3 Å molecular sieves. It was stored in the same Schlenk, protected from light, and kept under vacuum prior to use.

Electrochemistry. To avoid flocculation of the SWNTs, low concentrations of the supporting electrolyte were chosen to avoid any interference with the stability of the SWNT solution and minimize, at the same time, the electric resistance. The configuration and setting of the electrochemical cell is reported elsewhere.[44] The solvent was distilled by a trap-to-trap procedure into the electrochemical cell just before performing the electrochemical experiment. The pressure measured in the electrochemical cell prior to perform the trap-to-trap distillation of the solvent was typically around 1×10^{-5} mbar. Voltammograms were recorded with a custom-made fast potentiostat controlled by an AMEL model 568 function

(29) Scholes, G. D.; Rumbles, G. *Nat. Mater.* **2006**, *5*, 683.
(30) Spataru, C. D.; Ismail-Beigi, S.; Benedict, L. X.; Louie, S. G. *Phys. Rev. Lett.* **2004**, *92*, 077402.
(31) Chang, E.; Bussi, G.; Ruini, A.; Molinari, E. *Phys. Rev. Lett.* **2004**, *92*, 196401.
(32) Wang, F.; Dukovic, G.; Brus, L. E.; Heinz, T. F. *Science* **2005**, *308*, 838.
(33) Maultzsch, J.; Pomraenke, R.; Reich, S.; Chang, E.; Prezzi, D.; Ruini, A.; Molinari, E.; Strano, M. S.; Thomsen, C.; Lienau, C. *Phys. Rev. B* **2005**, *72*, 241402.
(34) Kiowski, O.; Lebedkin, S.; Hennrich, F.; Malik, S.; Rösner, H.; Arnold, K.; Sürgers, C.; Kappes, M. M. *Phys. Rev. B* **2007**, *75*, 075421.
(35) Dukovic, G.; Wang, F.; Song, D.; Sfeir, M. Y.; Heinz, T. F.; Brus, L. E. *Nano Lett.* **2005**, *5*, 2314.
(36) Wang, Z.; Pedrosa, H.; Krauss, T.; Rothberg, L. *Phys. Rev. Lett.* **2007**, *98*, 019702.
(37) Miyauchi, Y.; Saito, R.; Sato, K.; Ohno, Y.; Iwasaki, S.; Mizutani, T.; Jiang, J.; Maruyama, S. *Chem. Phys. Lett.* **2007**, *442*, 394.
(38) Perebeinos, V.; Tersoff, J.; Avouris, P. *Phys. Rev. Lett.* **2004**, *92*, 257402.
(39) Yu, G.; Jia, Y; Dong, J. *Phys. Rev. B* **2007**, *76*, 125403.
(40) McDonald, T. J.; Svedruzic, D.; Kim, Y.-H.; Blackburn, J. L.; Zhang, S. B.; King, P. W.; Heben, M. J. *Nano Lett.* **2007**, *7*, 3528.
(41) Bockris, J. O'M.; Reddy, A. K. N. *Modern Electrochemistry, Ionics*; Plenum Press: New York, 1998; Vol. 1, Chapter 2.
(42) Trasatti, S. *Pure Appl. Chem.* **1986**, *58*, 955.
(43) Georgakilas, V.; Kordatos, K.; Prato, M.; Guldi, D. M.; Holzinger, M.; Hirsch, A. J. *Am. Chem. Soc.* **2002**, *124*, 760.
(44) Marcaccio, M.; Paolucci, F.; Paradisi, C.; Carano, M.; Roffia, S.; Fontanesi, C.; Yellowlees, L. J.; Serroni, S.; Campagna, S.; Balzani, V. *J. Electroanal. Chem.* **2002**, *532*, 99.

generator.[45] Data acquisition was performed by a Nicolet model 3091 digital oscilloscope interfaced to a PC. The minimization of ohmic drop was achieved through the positive feedback circuit implemented in the potentiostat.

Spectroelectrochemistry. Visible-NIR spectroelectrochemical experiments were carried out using a quartz OTTLE cell with a 0.03 cm path length. The working electrode was a Pt−Rh (90:10) gauze with an optical transparency of about 40%. All of the details about the spectroelectrochemical setup have been reported in ref 46. The potential was set using an AMEL model 552 potentiostat connected to an AMEL model 568 function generator. All the spectra were recorded by a Varian Cary 5 UV−vis−NIR spectrophotometer. The electrochemical impedance spectroscopy was carried out to measure the uncompensated solution resistance with an Autolab model PGSTAT 30 (ECO CHEMIE) instrument.

(45) Amatore, C.; Lefrou, C. J. *Electroanal. Chem.* **1992**, *324*, 33.
(46) Lee, S. M.; Kowallick, R.; Marcaccio, M.; McCleverty, J. A.; Ward, M. D. J. *Chem. Soc., Dalton Trans.* **1998**, 3443.

Acknowledgment. This work was performed with partial support from the University of Bologna, the University of Trieste, the Italian Ministry of University and Research, and in the framework of the GDR-I No. 2756 "Science and applications of nanotubes". Helpful discussions with E. Anglaret and R. Martel are gratefully acknowledged. A.P. thanks K. Schierholz (Nanoledge) for a gift of carbon nanotubes and the French National Research Agency (ANR) for support under grant TRICOTRA.

Supporting Information Available: Structure of ***f*-NT**; comparison of spectroscopic data for ***h*-NT** in SDS/D_2O and DMSO; spectroelectrochemical data and analysis for Na[***a*-NT**] as a function of potential. Experimental and calculated work functions for 16 different semiconducting SWNTs. Simulated spectra for ***h*-NT** and ***a*-NT** and comparison of reported LUMO energy values with calculated E_{red}. This material is available free of charge via the Internet at http://pubs.acs.org.

JA710625P